EXPERIMENTAL ANALYSIS OF VESSEL STRUCTURES FOR FAST REACTOR JOYO UNDER SHOCK LOADING

Y. ANDO, S. KONDO
Department of Nuclear Engineering, The Faculty of Engineering, University of Tokyo, Bunkyo-ku, Tokyo, Japan

O. KAWAGUCHI
Power Reactor and Nuclear Fuel Development Corporation, Akasaka, Tokyo, Japan

T. UCHIDA
Japan Atomic Energy Research Institute, Tokai-mura, Ibaragi, Japan

SUMMARY

The reactor containment system is composed of several barriers of the release of energy, missiles, and radioactivity. The primary containment is emphasized to contain the reactor core system during all normal, abnormal, and credible accident condition without permitting significant leakage to the secondary containment, and, under the explosive hypothetical accident conditions, to absorb and dissipate the explosive effect in the primary system to assure the capability of removing the decay heat from the damaged core. In designing the liquid metal cooled fast reactor vessel, the vessel head, and the primary coolant loop which constitute the primary containment, it is required to determine the dynamic response of these components to an explosive core disruptive accident postulated for the reactor.

One of the approaches used to satisfy this requirement is to perform simulation experiment to predict the reactor damage and containment potential. In this paper we will present the results of a series of tests using chemical high explosives and slow burning explosives to investigate the hydrodynamic and structural effects of an accidental load to $\frac{1}{5}$-$\frac{1}{10}$ simple scaled models of the Japan's experimental fast reactor JOYO. Based on these tests, the strain energy distribution between the lower part of vessel and the upper part of vessel and/or the hold-down bolts has been studied. Semi-empirical rationale to correlate radial strain of vessel with explosive energy has been obtained based on not only this series of experiments but also experiments performed by other groups.

The other approach now employed by many groups is to solve the basic dynamical equations of reactor system numerically. Based on the one-dimensional Newtonian models of various parts of reactor system, the code ARIAKE has been developed to extrapolate our experimental results rationally. Our simulation experiments have been analysed by this code and the analyses showed encouraging results to predict mechanical consequences of accident in reactor system.

1. Introduction

The principal purpose of the containment system for liquid metal cooled fast breeder reactor (LMFBR) is to contain energy, missiles, and radioactive materials to protect the health and the safety of the public and the operator. In Japan's experimental fast reactor JOYO, this object is met by providing a double containment system, in which the primary containment system is emphasized to contain the reactor core system during all normal, abnormal, and credible accident conditions, and under the hypothetical core explosion accident, to absorb and dissipate the explosive effect in the primary system without permitting significant leakage to the secondary containment so as to assure the capability of removing the decay heat from the damaged core. The primary containment system is composed of the reactor vessel, the vessel head, and the primary loop. In designing a LMFBR, therefore, it is required to know in some detail the effect on the different part of the reactor structure of various pressure loadings in the event of a hypothetical core explosive accident.

One of the approaches used to satisfy this requirement is to perform simulation experiment for understanding the mechanical damage on the reactor vessel structure resulting from the nuclear excursion(1) (2). Only part of the thermal energy generated in a nuclear excursion is available for performing work on the system. The hypothetical nuclear excursion accident of JOYO has been analysed by a modified version of AX-1 code(3) and MARS(4) and ARIAKE code(5) later. ARIAKE code can give the rate of mechanical energy release not only by the expanding fuel vapor but also by the sodium vapor explosion after the molten fuel coming into contact with the coolant(6). The mechanical work potential due to the hypothetical core explosion accident of JOYO reactor has a magnitude of 200 MW-sec.

Chemical explosives such as TNT have been used to simulate nuclear excursions in fast reactors. The equivalence between the nuclear excursion energy available to do mechanical damage and TNT was based on estimates from TNT underwater explosions(7) where 1 lb. of TNT releases 2 MW-sec of energy, of which ~ 50 % is in the form of a shock wave and ~ 50 % in highly compressed vapor. It has become clear, however, that the rate of energy release of TNT was far faster than that of the nuclear excursion and that the fraction of the shock wave energy was unrealistically large as compared with the nuclear excursion. These facts should be taken into account when the result of the simulation experiment based on TNT equivalence is applied to the design evaluation of the real system(8).

In this paper, the results of three series of simulation experiment for the 200 MW-sec JOYO hypothetical accident will be summarized and a brief discussion of the pressure loading effects on various part of the vessel structure such as the deformation of the reactor vessel, cover and cover hold-down bolts will be given .

2. Experimental

Three series of experiment have been performed using many simple 1/10- and several complex 1/5-scale models of JOYO reactor vessel. Pentolite has been used as explosive energy source in most cases, and slow explosives such as ME and M-2 have been used in several cases for comparison purpose. About 20 channel records of the pressure history measured by piezoelectric pressure pick up and the transient strain measured by strain gauge were obtained in each case. The distribution of residual strain and the other changes of vessel structure due to explosive load was measured also.

The first series of experiments was designed to obtain information on the reactor vessel response, energy partition among vessel, shield plug, and hold down bolts, magnitude of the strains, and, scaling. The simple 1/10-scale model S 12, of which configuration is shown in Figure 1, is mostly made of SUS 27, the same material as used in the reactor. However, because the stress-strain curves for stainless steel differ at the test temperature for the model (room temperature) and at the operating temperature of reactor (500° C), a few models made of SS 41 and a few models with thicker wall were tested also. 50 g of Pentolite is neccesary for the simulation of JOYO hypothetical core accident in a 1/10-scale model filled with water.

The principal results obtained in this series are summarized in the followings.

(1) The energy partition is shown in the initial column of Table 1. The plastic work absorbed by the vessels is about 30 % of total released energy and this fraction does not show strong dependence on the thickness of the wall. On the other hand, the work energy absorbed by plug hold-down bolts, is only a few percent of the total energy. Thus a large fraction of the explosive energy must be absorbed by the water in the form of heat.

(2) The radial strain of the vessel wall is approximately predicted by the semi-empirical formula derived by Wise and Proctor[9] except the case in which the weight of the explosive is small.

(3) The location of the rupture is limited in the neighborhood of the welding line. The average membrane strain is estimated to be above 15 % when the vessel begins rupturing, but the local strain at the rupture section could not be measured.

In the second series of experiment, two explosives with slower burning velocity were used to investigate the effects of the energy generation rate and its form on the mechanical energy absorption by the vessel structure. All tests were performed using the simple 1/10-scale model S 12 depicted in Figure 1. The specifications of the explosives and the obtained energy partition are shown in Table 1. M-2 explosive produces very little permanent gas and the expected peak pressure is very small. Figure 2 is a typical record obtained in the case of M-2 explosion. This figure indicates that the wall loading is too small to cause the residual stress to the vessel

even by the explosion of 500 g M-2, which generates the same energy as 90 g Pentolite. In Table 1, the maximum radial strains ε_{max} caused by the charge equivalent to 50 g Pentolite are presented for various types of test models. These figures indicate that, as for radial deformation, the damage potential of ME energy is equivalent to that of Pentolite energy. Qualitatively, the reduction of damage potential due to the relatively low burning velocity of ME is compensated by its larger permanent gas production per unit energy generation. It is reasonable to expect that the smaller the energy absorbed by lower part of the vessel become, the larger becomes the kinetic energy of water slug which strikes the plug. The results shown in Table 1, and Figure 3, however, indicate that the residual strain energies of plug bolts obtained in the case of ME and M-2 explosion are smaller than that obtained in the case of Pentolite explosion. This is probably due to the fact that, in the case of slow explosion, acceleration of water slug due to shock is small and the resistance force of the plug hold-down bolts is large enough to prevent the water slug from converting its kinetic energy into plastic energy of the bolts.

The purpose of the last series of experiments is to investigate the failure threshold of the vessel under shock loading and the effects of the thermal shield and the dip-plate on the energy absorption potential of the vessel structure. Various types of 1/10-scale model vessel with plug, circumferential constraint, and core support plate have been tested using Pentolite. The configurations of the test vessel are shown in Figure 1. As for the characteristics of failure, the general results are summarized as follows, based on the data presented in Table 2;

(1) All the failure of vessel occurs in the neighborhood of welding line.

(2) If the core support plate is absent, the failure occurs along the welding line of the lower hemispherical part of the vessel. On the other hand, if the core support plate is introduced in this vessel, the failure location is shifted to the neighborhood of the longitudinal welding line of the vessel.

(3) The maximum radial strain of the thin wall vessel at marginal containment condition, ε^m_{max} shows large fluctuation. On the other hand, the data for the thick wall vessel shows small fluctuation and can be divided into two groups. The vessel group which shows higher ε^m_{max} has not the circumferential welding part and the other group which shows lower ε^m_{max} has circumferential welding line above the circumferential constraint such as stiffener.

(4) If the core support plate is absent, ε^m_{max} shows drastic decrease when the thermal shield is introduced in the vessel.

(5) ε^m_{max} does not decrease considerably even if a circumferential constraint is added to the vessel.

(6) Various axial distributions of the radial strain of the vessel are

compared in Figure 4. From this Figure it can be expected that the maximum radial strain ε_{max} is appeared at the same level as the center of explosion, in each case where whatever circumferential constraint is used among those depicted in Figure 1. Furthermore, the relation between ε_{max} and the weight of explosive is not altered by the addition of various circumferential constraints.

Other important results obtained in this series are summarized as follow;

(1) The effect of the thermal shield on maximum radial strain ε_{max} was investigated experimentally by changing the thickness of it and it was found that the maximum radial strain of the vessel with thermal shield, $(\varepsilon_{max})_{ts}$, was obtained from ε_{max} for the same vessel without thermal shield by the equation

$$\int_0^{(\varepsilon_{max})_{ts}} \sigma_t(\varepsilon)d\varepsilon = \frac{R_w t_w \bar{\sigma}_w}{R_w t_w \bar{\sigma}_w + \sum_j R_j t_j \bar{\sigma}_j} \int_0^{\varepsilon_{max}} \sigma_t(\varepsilon)d\varepsilon = R_{ts} \int_0^{\varepsilon_{max}} \sigma_t(\varepsilon)d\varepsilon \qquad (1)$$

where $\sigma_t(\varepsilon)$ is stress-strain curve for wall material, $\bar{\sigma}_j$ and $\bar{\sigma}_w$ are the average stress of the j th thermal shield and the wall, and t_w, t_j and R_j are the thickness of vessel wall, the thickness of j th thermal shield, and the radius of j th thermal shield.

(2) The effectiveness of dip-plate in reducing the water slug energy was also investigated. It was found that the energy absorbed by plug bolts was about 1 % of the total explosion energy in the case without dip-plate, and that this energy was roughly equal to the total energy absorbed by plug bolts and dip-plate, in case the dip-plate was introduced. The deformation of the upper part of the vessel was also caused by water slug movement and it was found that this deformation was prevented completely by adding the dip-plate.

3. Derivation of Semi-Empirical Equation

It has been recognized that the formula derived by Wise and Proctor could not explain the maximum radial strain ε_{max} obtained in the case where weight of explosive charge is small. After investigation of their published work of Ref.(9), we have arrived at the conclusion that the applicability of their formula to our series of experiment was suspicious because the ratio of vessel inner radius R_i to wall thickness h, R_i/h, in our case was generally larger than that in Ref.(9) and the expected strain rate of the wall in our case was smaller than that of their case as we have exploded only 25 or 50 g Pentolite in one shot of 1/10-scale model test. So we formulate another semi-empirical formula based not only on our results but also on the results published in Ref.(9).

Firstly, it is hypothesized that I, the impulse absorbed by the vessel wall, is related to the free water impulse I_f by an efficiency factor function ξ such that

$$I = I_f / \xi \qquad (2)$$

and I_f is given by Cole [7] as

$$I_f = KW^{\frac{1}{3}}\left(\frac{W}{R_i}\right)^{\frac{1}{3}\beta} \tag{3}$$

where K and β are constants.

ξ is assumed as a function of R_i/h in Ref. [9]. However, it is known that ξ is also a function of the tensile constraint in the wall, so it is more appropriate to assume that ξ is a function of $R_i\sigma_s/h\bar{\sigma}$ or

$$\xi = \xi(R_i\sigma_s/h\bar{\sigma}) \tag{4}$$

where σ_s is a reference stress and $\bar{\sigma}$ is an average stress of the wall in the process of deformation. We use the linear relation for the stress-strain curve,

$$\sigma_t = \sigma_y + (\sigma_u(1+\varepsilon_u)-\sigma_y)\varepsilon/\varepsilon_u, \tag{5}$$

where σ_t, σ_y, and σ_u represent true, yield, and ultimate stress, and ε is instantaneous strain and ε_u ultimate strain respectively. Then $\bar{\sigma}$ is given as $\sigma_t(\varepsilon_{max/2})$ by eq. (5).

The radial deformation velocity of the wall v_o can be derived from the equation of motion for a unit length of cylinder

$$2R_i\int P(t)dt = 2R_iI = \frac{w}{g}(R_e^2-R_i^2)v_o, \tag{6}$$

where P(t) is a pressure loading on the wall, w, the wall weight density, and g, the acceleration due to gravity. The deformation energy density of the wall D_h is equal to the total initial kinetic energy of the ring. Thus we can write that

$$D_h = \frac{w}{2g}v_o^2 \tag{7}$$

For the case of gross plastic deformation occurring at rapid rate of loading, the stress σ in a strain-hardening steel is at least a function of the strain ε and the strain rate $\dot{\varepsilon}$. Based on these consideration, the deformation energy density is expressed as

$$D_h = \int_0^{\varepsilon}\sigma_t(\varepsilon')d\varepsilon'\psi_1(\dot{\varepsilon}_o), \tag{8}$$

where ψ_1 is some dimensionless function of the initial strain rate $\dot{\varepsilon}_o$.

The solution of eq. (6), (7), (8) yields

$$W = (\psi_1\psi_2(\frac{Kp}{K})^2 w\int\sigma_t(\varepsilon)d\varepsilon(R_e^2-R_i^2)^2)^{\frac{3}{2(\beta+1)}} \tag{9}$$

, where $\psi_2 = \xi^2/2gK_p^2 = \psi_2(R_i\sigma_s/h\bar{\sigma})$, (10)

and Kp is the value of K for Pentolite.

To evaluate ψ_1 and ψ_2, eq. (9) is modified in the form

$$\psi_1\psi_2 = (\frac{K}{Kp})^2\frac{0.275W^{2(\beta+1)/3}}{w\int\sigma_t(\varepsilon)d\varepsilon\ (R_e^2-R_i^2)^2} \tag{11}$$

where 0.275 is necessary to express ψ_2 in effective dimension of $in^2/lb^{2/3}ft$ though w, W, R and σ_t are expressed in g/cc, g, cm and kg/cm^2. It is noted that the right hand side of eq. (11) is known from experimental results and material properties.

The efficiency factor ξ is necessary for the evaluation of $\dot{\varepsilon}_o$, as $\dot{\varepsilon}_o$ is calculated by the equation

$$\dot{\varepsilon}_o = \frac{v_o}{R_i} = \frac{154200 W^{\frac{\beta+1}{3}}}{\xi w R_i (R_e^2 - R_i^2)} \left(\frac{K}{K_p}\right) \tag{12}$$

Based on the data in Ref. [9] ξ is evaluated to be

$$\xi = 1.22 \left(R_i \sigma_s / h \bar{\sigma}\right)^{0.248} \tag{13}$$

where σ_s is set to 30 kg/mm^2 and β is assumed to be 1.

For accurate evaluation of ψ_2, it is required to use experimental results with a constant ψ_1 or $\dot{\varepsilon}_o$. Because it is impossible to fulfill this requirement in our case, ψ_2 is evaluated based on the results which give $\dot{\varepsilon}_o$ in the narrow range, that is, between 1400 sec^{-1} and 4000 sec^{-1} where ample data exists for that purpose.

The best fitted curve is taken to be

$$\psi_2 = \gamma \left(R_i \sigma_s / h \bar{\sigma}\right)^{0.497} \tag{14}$$

where γ is a constant.

Finally, at a fixed value of $R\sigma_s/h\bar{\sigma}$, the dependence of ψ_1 on $\dot{\varepsilon}_o$ is evaluated

$$\begin{aligned} \psi_1 &= \delta \left(\frac{\dot{\varepsilon}_o}{1400}\right)^{0.347} && \dot{\varepsilon}_o < 1400 \ sec^{-1} \\ &= \delta && 1400 < \dot{\varepsilon}_o < 4000 \ sec^{-1} \end{aligned} \tag{15}$$

where δ is a constant. Combining eq. (14) and (15) $\psi_1\psi_2$ is given by

$$\begin{aligned} \psi_1\psi_2 &= 2.4 \times 10^{-5} \left(R_i \sigma_s / h \bar{\sigma}\right)^{0.497} \left(\frac{\dot{\varepsilon}_o}{1400}\right)^{0.347} && \varepsilon_o < 1400 sec^{-1} \\ &= 2.4 \times 10^{-5} \left(R_i \sigma_s / h \bar{\sigma}\right)^{0.497} && \varepsilon_o > 1400 sec^{-1} \end{aligned} \tag{16}$$

With $\psi_1\psi_2$ now completely defined in terms of $(R_i\sigma_s/h\bar{\sigma})$ and $\dot{\varepsilon}_o$, the relation between W and ε_{max} can be expressed in the form

$$W = \left(\frac{41.5 \times 10^{-5} (R_e^2 - R_i^2)^{1.653} K_p^{1.653}}{w^{-0.653} R_i^{0.347} K^{1.653}} \left(\frac{R_i \sigma_s}{h \sigma_t(\varepsilon_{max}/2)}\right)^{0.411} R_{ts} \int_0^{\varepsilon_{max}} \sigma_t(\varepsilon) d\varepsilon \right)^{0.908} \tag{17}$$

where β is set to 1 and R_{ts} is the blast reduction factor of thermal shield defined in eq. (1). If β is not equal 1, then the value 0.908 shoud be replaced by $1.815/(\beta+1)$. In Figure 5 experimental data is shown in ψ_1-$\dot{\varepsilon}_o$ plane. Large fluctuation is mostly caused by the data for small h vessel.

4. Conclusion

The hydrodynamic and structural response of the JOYO primary vessel structure has been determined experimentally using many simple 1/10-and three 1/5-scale complex models. The results of these test indicate that the structural integrity of the JOYO will be maintained after core explosion accident which releases 200 MW-sec work energy.

Based on the results obtained in these series of experiment, our continuing test program will be directed to the investigation of the failure mechanism and the behavior of individual internal components under various pressure loading conditions.

Acknowledgement

This work was performed under contracts between Power Reactor and Nuclear Fuel Development Corporation and Nuclear Safety Research Association. The authors wish to express their thanks to all the members of the Shock Structure Committee of NSRA for their useful discussions.

References

(1) REES,N,J.M., "Mechanical effects of core accidents", Proceedings of the International Conference on Engineering of Fast Reactors for Safe and Reliable Operation, Karlsruhe (1972).

(2) DENISE,R.P. et al., "Containment of fast breeder reactors-recent developments in analytical and experimental methods", ibid.

(3) OKRENT,D. et al., "AX-1, A computing program for coupled neutronics hydrodynamics calculations on IBM-704", ANL-5977 (1959).

(4) HIRAKAWA,N. "MARS, A two-dimensional excursion code", APDA-198, June (1967).

(5) KONDO,S. et al., "Fast reactor core meltdown accident and the reactor vessel response", Proceedings of the International Conference on Engineering of Fast Reactors for Safe and Reliable Operation, Karlsruhe (1972).

(6) HICKS,E.P., MENZIES,D.C., "Theoretical Studies on the Fast Reactor Maximum Accident", ANL-7120 (1965).

(7) COLE,R.H., "Underwater Explosions", Dover Pub.Inc., New York (1958).

(8) COWLER,M.S., HOSKIN,N.E., "Comparison of the pressure effects of energy release from nuclear excursions and chemical simulations", Proceedings of the International Conference on Engineering of Fast Reactors for Safe and Reliable Operation, Karlsruhe (1972).

(9) WISE,W.R., Proctor,J.F., "Explosion containment laws for nuclear reactor vessels", NOL-TR-63-140 (1965).

Table 1. The specifications of explosives and the principal results of experiments

Explosive		Pentolite	ME	M2
Density	(g/cm^3)	1.6	0.6	1.8
Total energy	(cal/g)	1.22	0.37	0.22
Gas Production	(l/kg)	860	980	17
Burning velocity	(m/s)	7500	2000	100
ε_{max}(%) SUS 27	3 mm	12.7(31%)		
	5 mm	7.3(29%)	8 (31%)	
SS 41	3.2 mm	10.0(28%)		0.2 %
	6 mm	5.5(29%)	7.2(38%)	
	9 mm		4.7(37%)	
$\frac{\text{Plug bolt energy}}{\text{Total energy}}$	(%)	1.55	0.52	0.24

Table 2. The failure location and failure strain of the various model vessels.

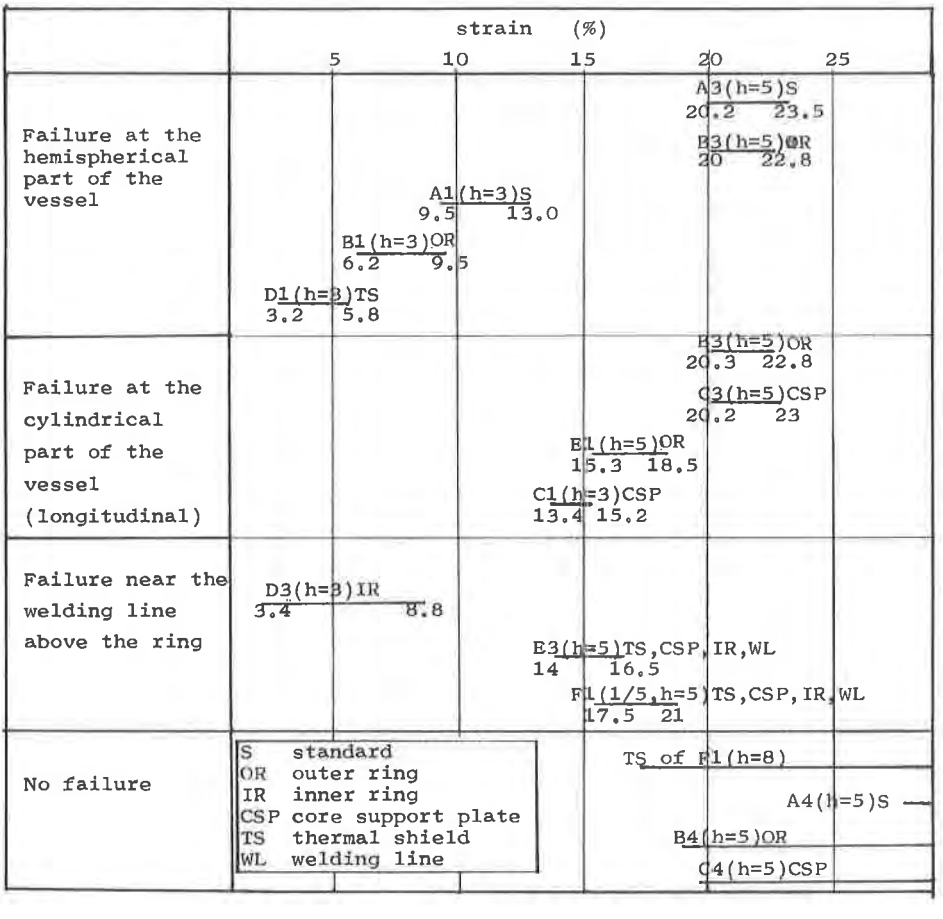

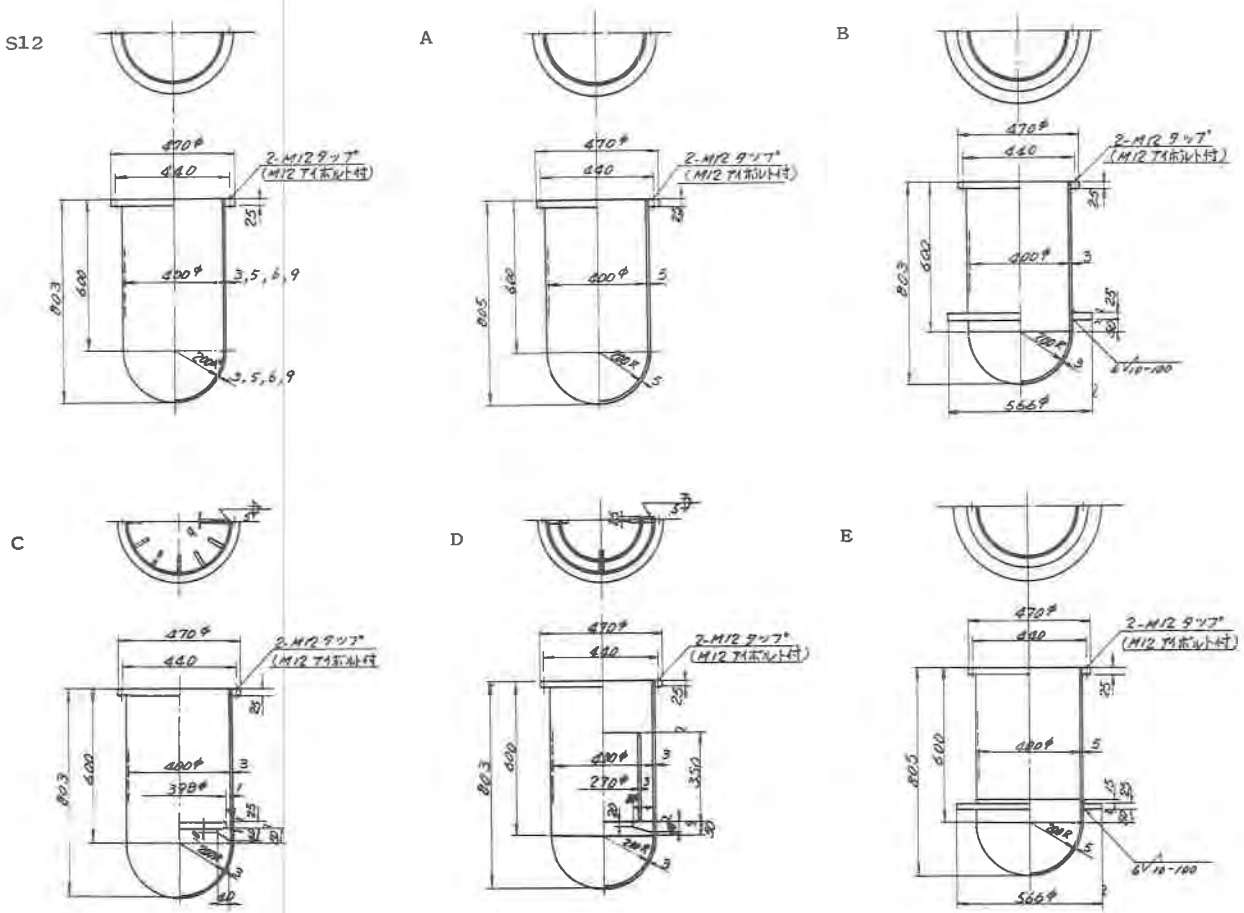

Figure 1. List of model vessels.

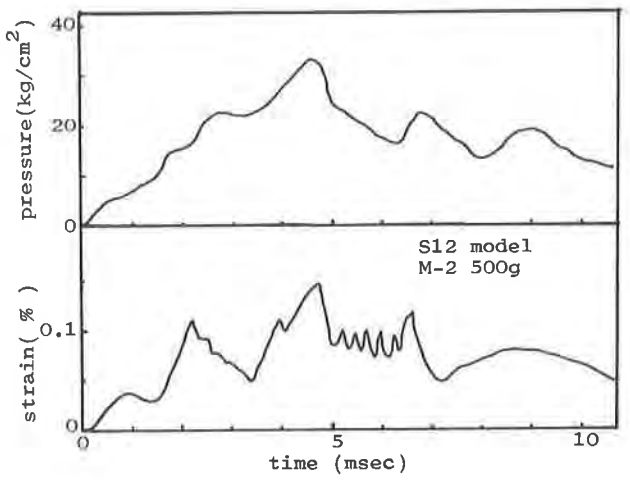

Figure 2. Typical pressure and strain history obtained M-2 explosion in 1/10 scale model test.

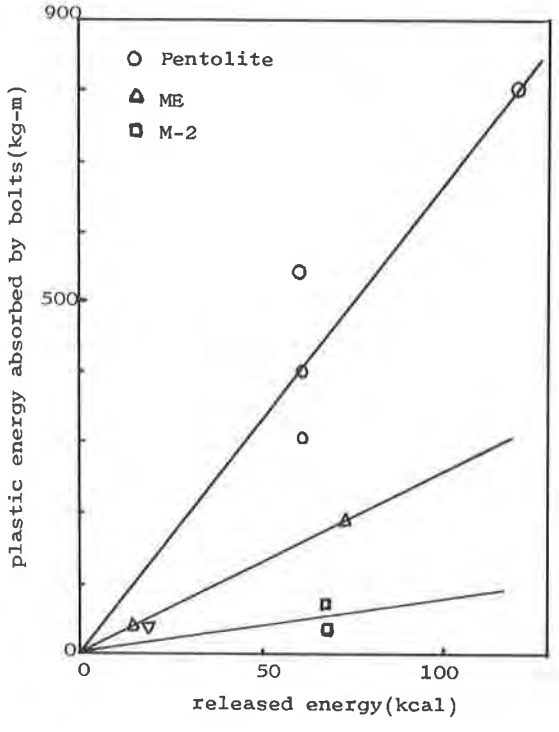

Figure 3. Plastic work energy absorbed by plug bolts vs. total released energy.

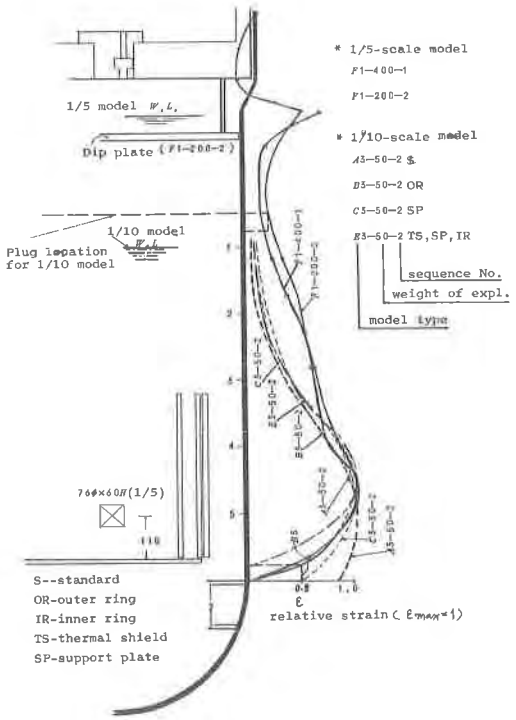

Figure 4. The axial distribution of radial strain of the vessel wall after Pentolite explosion in the various model tests.

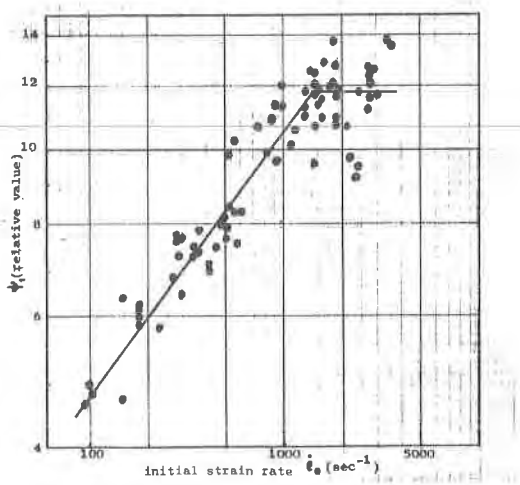

Figure 5. Variation of ψ_1 with initial strain rate $\dot{\varepsilon}_o$.